Theory of anchoring on a two-dimensionally grooved surface

Jun-ichi Fukuda,[1,2,*] Jin Seog Gwag,[2,†] Makoto Yoneya,[1,2] and Hiroshi Yokoyama[1,2]
[1]*Nanotechnology Research Institute, National Institute of Advanced Industrial Science and Technology (AIST), 1-1-1 Umezono, Tsukuba 305-8568, Japan*
[2]*Liquid Crystal Nano-System Project, ERATO/SORST, Japan Science and Technology Agency, 5-9-9 Tokodai, Tsukuba 300-2635, Japan*
(Received 20 June 2007; revised manuscript received 4 November 2007; published 10 January 2008)

We investigate analytically the anchoring of a nematic liquid crystal on a two-dimensionally grooved surface of arbitrary shape, induced by the elastic distortions of a liquid crystal adjacent to the surface. Our theoretical framework applied to a surface with square grooves reveals that such a surface can exhibit bistable anchoring, while a direct extension of a well-known theory of Berreman [Phys. Rev. Lett. **28**, 1683 (1972)] results in no azimuthal anchoring in the so-called one-constant case ($K_1=K_2=K_3$, with K_1, K_2, and K_3 being the splay, twist, and bend elastic constants, respectively). We show under the assumption of $K_1=K_2=K$ that the direction of the bistable easy axes and the anchoring strength crucially depend on the ratios K_3/K and K_{24}/K, where K_{24} is the saddle-splay surface elastic constant. To demonstrate the applicability of our theory to general cases and to elucidate the effect of surface shape and the elastic constants on the properties of surface anchoring, we also consider several specific cases of interest; one-dimensional grooves of arbitrary shape, rhombic grooves, and surfaces possessing $2N$-fold symmetry, including hexagonal grooves, and show the following: (i) The rescaled anchoring energy $f(\phi)/f(\pi/2)$ of one-dimensional grooves, with ϕ being the angle between the director $\boldsymbol{n}$ and the groove direction, is independent of the groove shape. (ii) Whether two diagonal axes of rhombic grooves can become easy axes depends sensitively on K_3/K, K_{24}/K and the angle α between the grooves. The angle α yielding the maximum anchoring strength for given groove pitch and amplitude depends again on K_3/K and K_{24}/K; in some cases $\alpha=0$ (one-dimensional grooves), and in other cases $\alpha\neq 0$, gives the maximum anchoring strength. Square grooves ($\alpha=\pi/2$) do not necessarily exhibit the largest anchoring strength. (iii) A surface possessing $2N$-fold symmetry can yield N-stable azimuthal anchoring. However, when $K_1=K_2=K_3$ and $N\geq 3$, azimuthal anchoring is totally absent irrespective of the value of K_{24}. The direction of the easy axes depends on K_3/K, K_{24}/K, and whether N is even or odd.

DOI: 10.1103/PhysRevE.77.011702 PACS number(s): 61.30.Hn, 61.30.Dk

I. INTRODUCTION

Surface anchoring of a liquid crystal [1–3] has been among the most important subjects of liquid crystal research. In most practical applications including displays, liquid crystals are confined in a cell made up of properly treated glass plates. Achievement of proper anchoring is of crucial importance in accomplishing desirable performance of liquid crystal devices.

The underlying mechanism of surface anchoring, together with how it can be controlled, has been also of fundamental interest. There has been a longstanding debate on what the origin of surface anchoring is, in particular on rubbed polymer surfaces. Intermolecular interactions between liquid crystal molecules and polymer chains constituting the surface have been identified as an important factor determining the anchoring properties [4–6]. On the other hand, elastic distortions of the liquid crystal adjacent to nonflat surfaces have long been argued as the source of surface anchoring as well, partly because of its universal nature irrespective of the chemical properties of the surface. The importance of the latter has been realized for the past decade because rapid progress in nanotechnology made it possible to create arbitrarily patterned or grooved surfaces with submicron-scale precision. Microscopically grooved surfaces have indeed been shown to exhibit anchoring in numerous experimental studies [7–15]. Anchoring properties realized by such surfaces include multistability [9,14], or controllable pretilt angle [10,11,15].

As early as in 1972, Berreman [16] presented the first theoretical study on surface anchoring attributed to nonflat surface geometry and the resultant elastic distortion of a nematic liquid crystal. With the assumption that the director $\boldsymbol{n}$ at the surface is always tangential to the surface, he discussed how the liquid crystal is distorted on and above a sinusoidally grooved surface. Since Berreman's work, although simple enough, captures the essence of surface anchoring induced by the elastic distortion of the liquid crystal, it has served as a starting point for subsequent numerous theoretical [17–20] as well as experimental [21–23] studies concerning the geometrical nature of surface anchoring.

However, in our recent work we argued that Berreman's theory is based on an invalid assumption of no azimuthal distortions of the director field [24]. Moreover, saddle-splay surface elasticity characterized by K_{24}, which does not appear in Berreman's theory because it becomes zero under the assumption of no azimuthal distortions, has been shown to play an important role [25,26]. The present understanding of the relation between anchoring and surface geometry based

*fukuda.jun-ichi@aist.go.jp
†Present address: Department Electronics and Computer Engineering, Hanyang University, 17 Haengdang-Dong, Seongdong-gu, Seoul 133-791, Korea.

on Berreman's argument must therefore be carefully and critically reexamined.

Our theory in Refs. [24–26], as well as the original version of Berreman's theory [16], was restricted to one-dimensionally grooved surfaces whose height is described by a single trigonometric function. Recently, as noted above, two-dimensionally patterned surfaces have been attracting interest as a type of anchoring surface. Therefore, it is worthwhile to investigate what kind of surface anchoring is induced by a nonflat surface of arbitrary shape, and how elastic constants including K_{24} affect the properties of such surface anchoring, which is the aim of the present paper.

There have been only a few theoretical studies to evaluate the anchoring properties of nonflat surfaces whose profiles cannot be described by a single trigonometric function. Bryan-Brown *et al.* [18] discussed the anchoring energy of an orthogonally grooved surfaces, but their argument, though essentially based on Berreman's original theory, did not contain the details of the derivation of their formula. Moreover, their anchoring energy implies that bistable azimuthal anchoring of square grooves appears only when $K_2 \neq K_3$ [see Eq. (3) for the definition of K_2 and K_3], which turns out to be wrong from our argument below. Elgeti and Schmid [20] avoided the invalid assumption of no azimuthal distortions to derive a general expression of the anchoring energy as a functional of the groove height. They did not, however, discuss specific cases of interest using their formula. We also notice that both Bryan-Brown *et al.* and Elgeti and Schmid paid no attention to the contribution of surface elasticity.

In Sec. II we derive the formula of the anchoring energy for an arbitrary surface profile. In Sec. III we apply our formula to several specific cases of interest; one-dimensional grooves of an arbitrary shape (Sec. III A), square grooves (Sec. III B), rhombic grooves (Sec. III C), and general grooves of $2N$-fold symmetry including hexagonal grooves (Sec. III D). We conclude this paper in Sec. IV.

II. THEORETICAL ARGUMENT

We consider a grooved surface whose height $\zeta(x,y)$ with respect to the plane $z=0$ is described by

$$\zeta(x,y) = \sum_{i=1}^{N} \zeta_i(x,y) \tag{1}$$

with

$$\zeta_i(x,y) = A_i \sin(\boldsymbol{q}_i \cdot \boldsymbol{r}_\perp + \varphi_i). \tag{2}$$

Here we have employed the abbreviation $\boldsymbol{r}_\perp = (x,y)$ and the wave number of the surface groove $\boldsymbol{q}_i = (q_{ix}, q_{iy})$ lies parallel to the $z=0$ plane. Without loss of generality, we can assume $\boldsymbol{q}_i \neq \boldsymbol{q}_j$ for $i \neq j$. Any $\zeta(x,y)$ can be expressed as a Fourier series (1) with Eq. (2), as long as $\zeta(x,y)$ is a single-valued, piecewise smooth and continuous function. When no periodicity in $\zeta(x,y)$ can be assumed, the sum $\Sigma_{i=1}^{N}$ in Eq. (1) and the following equations should be understood as an integral with respect to $\boldsymbol{q}$. We have denoted the amplitude of the groove by A_i, and φ_i characterizes the phase of the groove. We assume $A_i|\boldsymbol{q}_i| \ll 1$, that is, the slope of the groove is small enough.

A nematic liquid crystal is filled in a semi-infinite region $z > \zeta(x,y)$. We denote the average orientation of the nematic liquid crystal by the director $\boldsymbol{n}$, and the Frank elastic energy in terms of $\boldsymbol{n}$ is written as [1,27,28]

$$F = \frac{1}{2}\int d\boldsymbol{r}[K_1(\boldsymbol{\nabla}\cdot\boldsymbol{n})^2 + K_2(\boldsymbol{n}\cdot\boldsymbol{\nabla}\times\boldsymbol{n})^2 + K_3(\boldsymbol{n}\times\boldsymbol{\nabla}\times\boldsymbol{n})^2 - K_s\boldsymbol{\nabla}\cdot(\boldsymbol{n}\boldsymbol{\nabla}\cdot\boldsymbol{n} + \boldsymbol{n}\times\boldsymbol{\nabla}\times\boldsymbol{n})]. \tag{3}$$

Here K_1, K_2, and K_3 are the bulk elastic constants associated with splay, twist, and bend deformations, respectively. The last term in Eq. (3) is referred to as the surfacelike elastic term because it is converted to a surface integral. We have introduced $K_s \equiv K_2 + K_{24}$, where K_{24} is the saddle-splay elastic constant [27–29].

Here we do not consider the term $K_{13}\boldsymbol{\nabla}\cdot(\boldsymbol{n}\boldsymbol{\nabla}\cdot\boldsymbol{n})$, because this term renders the problem of finding the profile of $\boldsymbol{n}$ minimizing F ill-defined [27,30], and even the existence of this term has been questioned [31].

From their molecular theory, Nehring and Saupe [29] showed a relation $K_{24} = (K_1 - K_2)/2$, or $K_s = (K_1 + K_2)/2$. However, experimental measurements do not seem to support it [32], and Yokoyama [31] argued that this equality should be replaced by an inequality

$$K_{24} \geq (K_1 - K_2)/2 \quad \text{or} \quad K_s \geq (K_1 + K_2)/2. \tag{4}$$

Therefore, in the following, we treat K_s or K_{24} as an independent parameter. We also notice that for the elastic energy F to be positive-definite,

$$K_3 \geq 0, \quad 0 \leq K_s \leq 2K_1, \quad K_s \leq 2K_2 \tag{5}$$

must be fulfilled [28,33].

We assume uniform alignment at infinity, $z = +\infty$, and take the x direction parallel to $\boldsymbol{n}$ at $z = +\infty$. When the distortion of the nematic liquid crystal from the uniform alignment along the x direction is small enough, it is characterized by n_y and n_z that satisfy $|n_y| \ll 1$ and $|n_z| \ll 1$. Then we are allowed to retain up to second-order terms in n_y and n_z in the Frank elastic energy, which reads as

$$F = \frac{1}{2}\int d\boldsymbol{r}\{K_1(\partial_y n_y + \partial_z n_z)^2 + K_2(\partial_y n_z - \partial_z n_y)^2 + K_3[(\partial_x n_y)^2 + (\partial_x n_z)^2] - 2K_s(\partial_y n_y \partial_z n_z - \partial_y n_z \partial_z n_y)\}. \tag{6}$$

We assume planer degenerate anchoring at the grooved surface; i.e., the director $\boldsymbol{n}$ is always perpendicular to the surface normal ν, but there is no preferred direction as long as $\boldsymbol{n}\cdot\nu = 0$ is fulfilled. Since $\nu \| (\partial\zeta/\partial x, \partial\zeta/\partial y, -1)$, the condition of planar degenerate anchoring at the surface is explicitly written as

$$\frac{\partial\zeta}{\partial x} + n_y\frac{\partial\zeta}{\partial y} - n_z = 0. \tag{7}$$

As we discussed in our previous study [24], Eq. (7) does not give any boundary condition for n_y because $n_y \partial\zeta/\partial y$ gives a contribution higher order in $A_i|\boldsymbol{q}_i|$. The leading-order term in Eq. (7) yields a boundary condition for n_z that reads

$$n_z = \frac{\partial \zeta}{\partial x} = \sum_{i=1}^{N} A_i q_{ix} \cos(\boldsymbol{q}_i \cdot \boldsymbol{r}_\perp + \varphi_i). \tag{8}$$

We also showed [24] that the variational principle applied to the Frank elastic energy (6) yields the Euler-Lagrange equations in the bulk:

$$0 = -K_1 \partial_y (\partial_y n_y + \partial_z n_z) + K_2 \partial_z (\partial_y n_z - \partial_z n_y) - K_3 \partial_x^2 n_y, \tag{9}$$

$$0 = -K_1 \partial_z (\partial_y n_y + \partial_z n_z) - K_2 \partial_y (\partial_y n_z - \partial_z n_y) - K_3 \partial_x^2 n_z, \tag{10}$$

together with an additional boundary condition at the surface [25,26],

$$K_s \partial_y n_z + K_2 (\partial_z n_y - \partial_y n_z) = 0. \tag{11}$$

The derivation of Eqs. (9) and (10) is straightforward. Equation (11) arises from the fact that n_z at the boundary is fixed [see Eq. (8)], that is, infinitesimal variation of n_z is not allowed; $\delta n_z = 0$. On the other hand, as mentioned above, no condition is imposed on n_y at the surface, i.e., $\delta n_y \neq 0$.

Thus, to find the equilibrium director profile at and above the grooved surface, we must solve Eqs. (9) and (10) under the boundary conditions (8) and (11). Since those equations are linear in n_y and n_z, superposition principle is readily applied; when the solution for the surface described by one sinusoidal mode is known, the final solution is given just by the sum of those individual solutions. We already know that when Eq. (8) is replaced by a single sinusoidal function, $n_z = A_i q_{ix} \cos(\boldsymbol{q}_i \cdot \boldsymbol{r}_\perp + \varphi_i)$, the solution is represented, in the present terminology, by [25,26]

$$n_z^{(i)} = A_i q_{ix} \cos(\boldsymbol{q}_i \cdot \boldsymbol{r}_\perp + \varphi_i) \left(e^{-k_i^{(1)} z} + \frac{K_s}{K_3} \frac{q_{iy}^2}{q_{ix}^2} (e^{-k_i^{(1)} z} - e^{-k_i^{(2)} z}) \right), \tag{12}$$

$$n_y^{(i)} = A_i q_{ix} \sin(\boldsymbol{q}_i \cdot \boldsymbol{r}_\perp + \varphi_i) \left[\frac{q_{iy}}{k_i^{(1)}} e^{-k_i^{(1)} z} + \frac{K_s}{K_3} \frac{q_{iy}^2}{q_{ix}^2} \times \left(\frac{q_{iy}}{k_i^{(1)}} e^{-k_i^{(1)} z} - \frac{k_i^{(2)}}{q_{iy}} e^{-k_i^{(2)} z} \right) \right], \tag{13}$$

where we have defined $k_i^{(j)} \equiv \sqrt{q_{iy}^2 + (K_3/K_j) q_{ix}^2}$ $(j = 1, 2)$. We note that Eqs. (12) and (13) have been already derived by Wolff *et al.* [34], although they did not discuss the explicit form of the anchoring energy we shall give below, and their argument was restricted to one-dimensional grooves. As noted above, the final solution to Eqs. (9) and (10) under the boundary conditions (8) and (11) is expressed as $n_z = \Sigma_i n_z^{(i)}$, and $n_y = \Sigma_i n_y^{(i)}$.

Substituting the obtained director profile into Eq. (6), we find the Frank elastic energy due to the distortion induced by the grooved surface, or the anchoring energy of the grooved surface. Here again the superposition principle can be applied, and the resultant anchoring energy is

$$f = \frac{1}{4} \sum_{i=1}^{N} A_i^2 \frac{q_{ix}^2}{k_i^{(1)}} \left[(K_3 q_{ix}^2) + K_s q_{iy}^2 \left(2 - \frac{K_s}{K_3} \frac{k_i^{(1)} k_i^{(2)} - q_{iy}^2}{q_{ix}^2} \right) \right], \tag{14}$$

per unit surface area.

Equation (14) is a complicated function to deal with analytically. Therefore, in some of the following discussions, we make a simplifying assumption, $K_1 = K_2 = K$. Then Eq. (14) reads as

$$f = \frac{1}{4} \sum_{i=1}^{N} A_i^2 \frac{q_{ix}^2}{k_i^{(1)}} \left[K_3 q_{ix}^2 + K_s \left(2 - \frac{K_s}{K} \right) q_{iy}^2 \right]. \tag{15}$$

Equation (15), or (14), serves as a starting point in the following discussions on the anchoring properties of various surfaces.

III. DISCUSSION

In this section, using the anchoring energy derived in the preceding section, we discuss several specific cases of interest; one-dimensional grooves with arbitrary shape, square grooves, rhombic grooves, and two-dimensional grooves with $2N$-fold symmetry including hexagonal grooves.

A. One-dimensionally grooved surface with arbitrary shape

Height profiles of any one-dimensionally grooved surface can be described in terms of Fourier series with wave vectors pointing along the same direction perpendicular to the grooves. We denote such a set of parallel wave vectors as $\{\boldsymbol{q}_i\} = \{q_i(\sin\phi, \cos\phi)\}$, in which ϕ describes the angle between the uniform director $\boldsymbol{n}$ at infinity and the direction of the groove. Here we do not assume $K_1 = K_2$ and the anchoring energy, Eq. (14), is rewritten as

$$f = \frac{1}{4} \left(\sum_{i=1}^{N} A_i^2 q_i^3 \right) \left[K_3 \frac{\sin^4 \phi}{g_1(\phi)} + K_s \frac{\cos^2 \phi \sin^2 \phi}{g_1(\phi)} \times \left(2 - \frac{K_s}{K_3} \frac{g_1(\phi) g_2(\phi) - \cos^2 \phi}{\sin^2 \phi} \right) \right], \tag{16}$$

where we have defined $g_i(\phi) = \sqrt{\cos^2 \phi + (K_3/K_i) \sin^2 \phi}$ $(i = 1, 2)$. Since in Eq. (16) the shape of the surface enters only through the sum $\Sigma_{i=1}^{N} A_i^2 q_i^3$, the reduced anchoring energy $f(\phi)/f(\phi = \pi/2)$ is independent of the shape of the surface.

The surface anchoring energy in the literature is often written in a Rapini-Papoular form as [35] $f = (1/2) W \sin^2 \phi$ or $f = (1/2) W \phi^2$ for small ϕ. From Eq. (16), we have

$$W = \frac{1}{2} \left(\sum_{i=1}^{N} A_i^2 q_i^3 \right) K_s \left(2 - \frac{1}{2} K_s \frac{K_1 + K_2}{K_1 K_2} \right). \tag{17}$$

From Eq. (17), we find that surfacelike elasticity plays a decisive role in the Rapini-Papoular anchoring strength W, and W vanishes when the contribution from the surfacelike elasticity is absent $(K_s = 0)$, or $K_s = 4K_1 K_2/(K_1 + K_2)$. To see the effect of surfacelike elasticity, we plot in Fig. 1 the reduced anchoring energy $f(\phi)/f(\pi/2)$ for various K_s. In Fig.

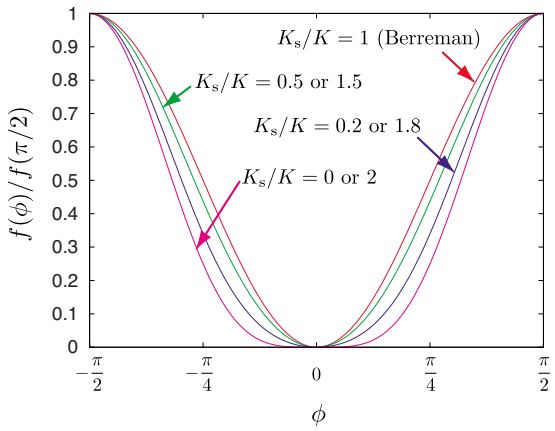

FIG. 1. (Color online) Plot of the reduced anchoring energies $f(\phi)/f(\pi/2)$ for various K_s. Here we assume $K_1=K_2=K_3=K$.

1 we have considered a simplified one-constant case $K_1=K_2=K_3=K$. The absence of surface anchoring in the Rapini-Papoular sense in the case of $K_s=0$ or $2K$ is clearly seen, and the original result of Berreman, $f(\phi)\propto\sin^2\phi$, is recovered when $K_s=K$ [26].

B. Surface with square grooves

We consider a surface with two-dimensional grooves of square shape. The surface profile can be described using two orthogonal wave vectors of equal length, i.e., $\boldsymbol{q}_1$ and $\boldsymbol{q}_2$ with $\boldsymbol{q}_1\cdot\boldsymbol{q}_2=0$ and $|\boldsymbol{q}_1|=|\boldsymbol{q}_2|=q$. We set the amplitude of those orthogonal grooves to be equal, that is, $A_1=A_2=A$. We again introduce an angle ϕ characterizing the direction of one of the orthogonal grooves with respect to $\boldsymbol{n}$, and write $\boldsymbol{q}_{1,2}$ as $\boldsymbol{q}_1=q(\sin\phi,\cos\phi)$ and $\boldsymbol{q}_2=q(\cos\phi,-\sin\phi)$. The geometry of our setup is illustrated in Fig. 2.

Here we discuss a simplified case with $K_1=K_2=K$ and define $k_3\equiv K_3/K$ and $k_s\equiv K_s/K$. The inequality (5) now reads $k_3\geq 0$ and $0\leq k_s\leq 2$. The anchoring energy, Eq. (15), then reads as

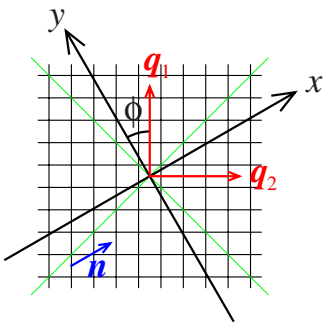

FIG. 2. (Color online) Illustration of the geometry of the square grooves. Thin green lines represent the direction of easy axes ($\phi=\pi/4, 3\pi/4$). The angle ϕ can be understood as the angle between the director $\boldsymbol{n}$ (or the x axis) and the direction of one of the grooves (represented by thin solid black lines), as well as the angle between $\boldsymbol{q}_1$ and the y axis.

$$f=\frac{1}{4}KA^2q^3\left(\frac{k_3\sin^4\phi+k_s(2-k_s)\cos^2\phi\sin^2\phi}{\sqrt{\cos^2\phi+k_3\sin^2\phi}}+\frac{k_3\cos^4\phi+k_s(2-k_s)\sin^2\phi\cos^2\phi}{\sqrt{\sin^2\phi+k_3\cos^2\phi}}\right). \tag{18}$$

Obviously, the value of f for given k_3 and ϕ is the same for $k_s=1\pm\alpha$, where $|\alpha|\leq 1$. Therefore, unless otherwise stated, we will restrict our discussion to $k_s\geq 1$ [which is also consistent with Eq. (4)]. From Eq. (18), one readily finds that $\partial f/\partial\phi=0$ at $\phi=n\pi/4$, with n being an arbitrary integer. Now we discuss whether f attains its local minimum or maximum at $\phi=n\pi/4$. We define $W(\phi)\equiv\partial^2 f/\partial\phi^2$. When $\partial f/\partial\phi=0$ and $W(\phi)>0$, the angle ϕ becomes stable (or metastable). From Eq. (18), we find

$$W(0)=\frac{1}{4}KA^2q^3\left(2k_s(2-k_s)+\frac{2k_s(2-k_s)-(3k_3+1)}{\sqrt{k_3}}\right), \tag{19}$$

$$W(\pi/4)=\frac{1}{4}KA^2q^3\frac{1}{\sqrt{2}(1+k_3)^{5/2}}[k_3(3k_3^2+10k_3+19)-k_s(2-k_s)(5k_3^2+22k_3+5)]. \tag{20}$$

It is obvious from symmetry that $W(0)=W(m\pi/2)$ and $W(\pi/4)=W(\pi/4+m\pi/2)$, with m being an arbitrary integer. From cumbersome calculations we do not present here, it can be shown that $W(0)>0$ and $W(\pi/4)>0$ cannot be simultaneously satisfied. Therefore, apart from the special cases with $W(0)=0$ or $W(\pi/4)=0$, we must consider the following three cases: (i) $W(0)<0$ and $W(\pi/4)>0$, (ii) $W(0)>0$ and $W(\pi/4)<0$, and (iii) $W(0)<0$ and $W(\pi/4)<0$. In cases (i) and (ii) our system becomes stable when $\phi=\pi/4$ and $\phi=0$, respectively. Two easy axes are thus along the diagonal directions in case (i), and along the sides of squares in case (ii). In case (iii), one can show that there exists an angle ϕ_i in the range $(0,\pi/4)$ which satisfies $W(\phi_i)=0$. The minima of the anchoring energy f are then located at $\phi=\pm\phi_i+m\pi/2$, and therefore the system has four easy axes along $\phi=\pm\phi_i$ and $\pi/2\pm\phi_i$ [36].

To see which case happens for given k_3 and k_s, we plot a phase diagram in Fig. 3, together with schematic illustrations of the easy axes for cases (i), (ii), and (iii). We find from Fig. 3 that when $k_3>1$, case (i) is always realized, and thus the easy directions are along the diagonal directions. When $k_3<1$, which case holds depends on k_s, and for $k_s=1$, we observe case (ii) for all $k_3<1$. Case (iii) is found in a very narrow region in the phase diagram. We note that for most of the rodlike nematic liquid crystals, K_3 is larger than K_1 and K_2 [1], and therefore $k_3>1$. Hence, in most practical situations case (i) is likely to be observed.

We notice also that Berreman's original theory corresponds to choosing $k_s=1$ as noted in Ref. [26] and Sec. III A. In the one-constant case ($k_3=1$) together with $k_s=1$, one can easily find from Eq. (18) that the anchoring energy becomes $f=(1/4)KA^2q^3(\cos^2\phi+\sin^2\phi)^2=$const. Thus, in the case of $k_3=1$ and $k_s=1$ (marked by a dot in Fig. 3), no azimuthal anchoring is present, or in other words, naive extension of

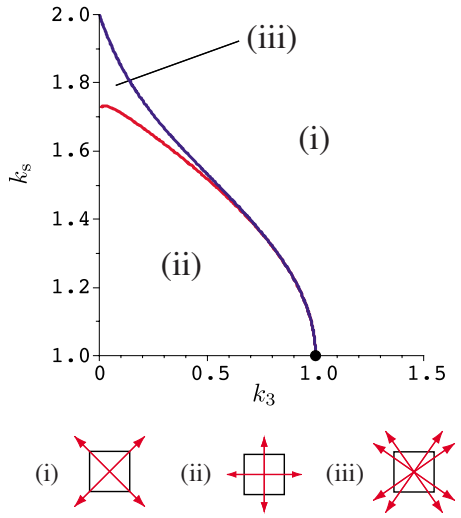

FIG. 3. (Color online) Phase diagram of a surface with square grooves. Schematic illustrations of the easy axes are also given. At the point ($k_3=1$, $k_s=1$) marked by a dot, no azimuthal anchoring is present.

Berreman's theory to square grooves results in no azimuthal anchoring in the one-constant case ($K_1=K_2=K_3$), This marks a sharp contrast to our result accounting for azimuthal anchoring even in the one-constant case unless $k_s=1$.

We further comment that the result of Bryan-Brown *et al.* [Eq. (2) of Ref. [18]] in the case of square grooves is equal to our Eq. (18) when $K_1=K_2$ and $k_s=1$. However, when $K_1 \neq K_2$, their result does not agree with what is expected from our general formula, Eq. (14), whichever K_s is chosen. Considering the additional fact that surface elasticity does not appear in their argument, we conclude that the derivation of the anchoring energy by Bryan-Brown *et al.* [18] is based on some erroneous argument.

To observe the behavior of the anchoring energy in a clearer manner, In Fig. 4, we plot the ϕ dependence of the anchoring energy for various k_3 and k_s. For the clarity of the presentation, we have introduced a rescaled anchoring energy $\tilde{f}(\phi)$ defined by

$$\frac{1}{4}KA^2q^3\tilde{f}(\phi) = f(\phi) - \frac{1}{2\pi}\int_0^{2\pi} f(\phi). \tag{21}$$

For $k_3=1.5>1$ [Fig. 4(a)], the minima are located at $\phi=\pi/4$ and $3\pi/4$ [corresponding to case (i)], irrespective of the value of k_s. On the other hand, for $k_3=0.7<1$ [Fig. 4(b)], the position of the minima depends on k_s; when $k_s=1$ they are located at $\phi=0$ and $\pi/2$, while for other values of k_s at $\phi=\pi/4$ and $3\pi/4$. Figure 4(c) corresponds to case (iii), in which $\phi=0$ and $\phi=\pi/4$ are at the local maximum of $\tilde{f}$ and the minima are found in between. Those behaviors are in agreement with the phase diagram, Fig. 3.

To conclude this section we notice from Eq. (20) that the anchoring strength $W(\pi/4)$ in case (i) for fixed k_3 is the largest when $k_s=2$ (or 0). On the other hand, in case (ii) ($k_3<1$) the largest anchoring strength $W(0)$ [Eq. (19)] is

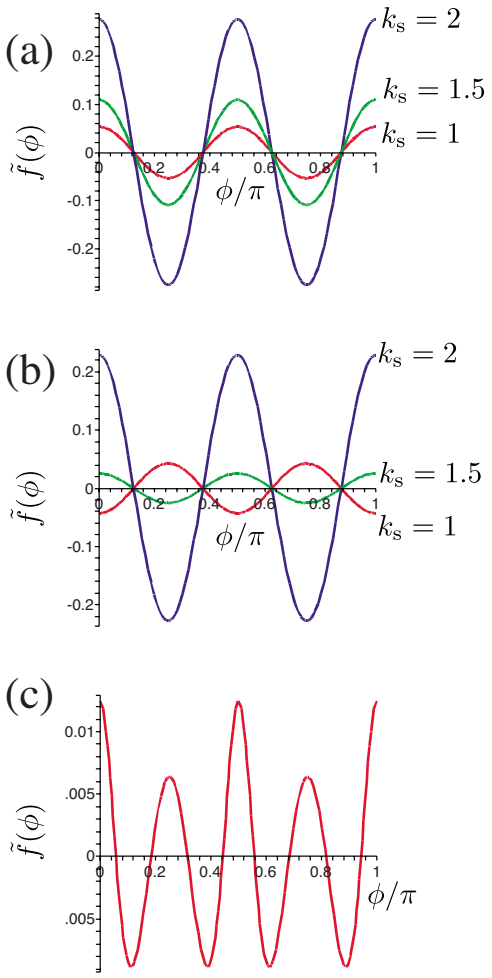

FIG. 4. (Color online) Plot of the rescaled anchoring energy $\tilde{f}(\phi)$ for (a) $k_3=1.5$, (b) $k_3=0.7$, and (c) $k_3=0.1$ and $k_s=1.8$.

achieved when $k_s=1$. The plot of the anchoring strengths $W(0)$ and $W(\pi/4)$ as a function of k_3 and k_s in Fig. 5, as well as the behavior of the anchoring energy in Fig. 4, agrees with the argument above.

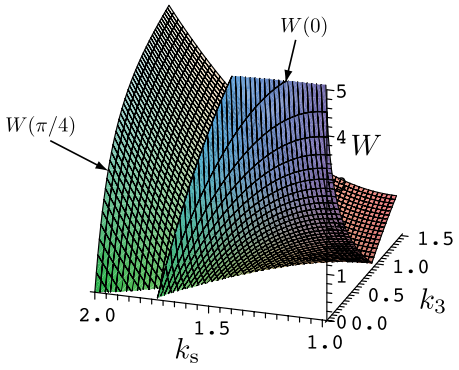

FIG. 5. (Color online) Plot of the anchoring strengths $W(0)$ and $W(\pi/4)$ as a function of k_3 and k_s for a surface with square grooves. Only the regions where $W(0)>0$ or $W(\pi/4)>0$ are shown.

C. Surface with rhombic grooves

We discuss here the properties of anchoring on a surface with nonorthogonal grooves. We restrict our discussion to two-dimensional grooves with equal pitch ($|\boldsymbol{q}_1|=|\boldsymbol{q}_2|=q$) and amplitude ($A_1=A_2=A$). Therefore, we consider grooves with rhombic shape. We denote the angle between grooves by α and then $\boldsymbol{q}_1\cdot\boldsymbol{q}_2=q^2\cos\alpha$. The square grooves discussed in Sec. III B correspond to the case with $\alpha=\pi/2$. Without loss of generality, we can impose the condition $0\leq\alpha\leq\pi/2$.

We again let ϕ describe the direction between one of the grooves and $\boldsymbol{n}$, and then the wave vectors $\boldsymbol{q}_{1,2}$ are written as $\boldsymbol{q}_1=q(\sin\phi,\cos\phi)$ and $\boldsymbol{q}_2=q[\sin(\phi-\alpha),\cos(\phi-\alpha)]$ (note that the definition of $\boldsymbol{q}_2$ is different from that in Sec. III B; the present definition corresponds to $-\boldsymbol{q}_2$ in Sec. III B). Figure 6 illustrates the geometry of the present setup.

For the clarity of the following argument, we introduce a different angle $\tilde{\phi}=\phi-\alpha/2$, which can be understood as an angle between $\boldsymbol{n}$ and one of the diagonal lines of the rhombi. Again after a simplifying assumption of $K_1=K_2=K$, the anchoring energy (14) becomes

$$f=\frac{1}{4}KA^2q^3\left(\frac{k_3\sin^4\left(\tilde{\phi}+\frac{\alpha}{2}\right)+k_s(2-k_s)\cos^2\left(\tilde{\phi}+\frac{\alpha}{2}\right)\sin^2\left(\tilde{\phi}+\frac{\alpha}{2}\right)}{\sqrt{\cos^2\left(\tilde{\phi}+\frac{\alpha}{2}\right)+k_3\sin^2\left(\tilde{\phi}+\frac{\alpha}{2}\right)}}+\frac{k_3\sin^4\left(\tilde{\phi}-\frac{\alpha}{2}\right)+k_s(2-k_s)\cos^2\left(\tilde{\phi}-\frac{\alpha}{2}\right)\sin^2\left(\tilde{\phi}-\frac{\alpha}{2}\right)}{\sqrt{\cos^2\left(\tilde{\phi}-\frac{\alpha}{2}\right)+k_3\sin^2\left(\tilde{\phi}-\frac{\alpha}{2}\right)}}\right). \tag{22}$$

Here again $k_3\equiv K_3/K$ and $k_s\equiv K_s/K$. It is easy to verify that at $\tilde{\phi}=n\pi/2$ or $\phi=n\pi/2+\alpha/2$ (with n being an integer), $\partial f/\partial\phi=\partial f/\partial\tilde{\phi}=0$. It is important to notice, however, that it does not imply that the extrema of f are found only at $\tilde{\phi}=n\pi/2$; as we have seen in Sec. III B, for $\alpha=\pi/2$, $\partial f/\partial\phi=0$ at $\phi=n\pi/2$ ($\tilde{\phi}=n\pi/2-\pi/4$) as well as at $\phi=n\pi/2+\pi/4$ ($\tilde{\phi}=n\pi/2$).

Since the anchoring energy (22) is still a highly complicated function of $\tilde{\phi}$, k_3, k_s, and α, we will restrict our discussion here to whether the axes $\tilde{\phi}=0$ and $\tilde{\phi}=\pi/2$ along the diagonal directions are stable (metastable) or unstable. We note that when both $\tilde{\phi}=0$ and $\tilde{\phi}=\pi/2$ are unstable, there should be easy axes along different directions as in the cases (ii) and (iii) in the preceding section. In those cases, with the values of k_3, k_s, and α fixed, we can calculate the direction $\tilde{\phi}$ of the easy axes numerically, which we will not do here.

In the present case, $W(\tilde{\phi})=\partial^2 f/\partial\tilde{\phi}^2$ at $\tilde{\phi}=0$ becomes

$$\begin{aligned}W(0)=\frac{\frac{1}{4}KA^2q^3}{\left(\cos^2\frac{\alpha}{2}+k_3\sin^2\frac{\alpha}{2}\right)^{5/2}}\Bigg[&2k_3\sin^2\frac{\alpha}{2}\Bigg(12+(15k_3-31)\\&\times\sin^2\frac{\alpha}{2}+2(k_3-1)(3k_3-14)\sin^4\frac{\alpha}{2}\\&-9(k_3-1)^2\sin^6\frac{\alpha}{2}\Bigg)+2k_s(2-k_s)\Bigg(2-(k_3+15)\sin^2\frac{\alpha}{2}\\&-(17k_3-33)\sin^4\frac{\alpha}{2}-(k_3-1)(7k_3-29)\sin^6\frac{\alpha}{2}\\&+9(k_3-1)^2\sin^8\frac{\alpha}{2}\Bigg)\Bigg].\end{aligned} \tag{23}$$

We note that $W(0,\alpha)=W(\pi/2,\pi-\alpha)$ from symmetry, or equivalently,

$$W[0,\sin(\alpha/2)]=W[\pi/2,\cos(\alpha/2)]. \tag{24}$$

For the following discussion, we also present the values of $W(0)$ at $k_s=0$, 1, and 2:

$$\begin{aligned}W(0)|_{k_s=0\text{ or }2}=&\frac{\frac{1}{4}KA^2q^3}{\left(\cos^2\frac{\alpha}{2}+k_3\sin^2\frac{\alpha}{2}\right)^{5/2}}\\&\times2k_3\sin^2\frac{\alpha}{2}\Bigg[3\sin^4\frac{\alpha}{2}\left(2-3\sin^2\frac{\alpha}{2}\right)k_3^2\\&+\sin^2\frac{\alpha}{2}\left(18\sin^4\frac{\alpha}{2}-34\sin^2\frac{\alpha}{2}+15\right)k_3\\&+\left(-9\sin^6\frac{\alpha}{2}+28\sin^4\frac{\alpha}{2}-31\sin^2\frac{\alpha}{2}+12\right)\Bigg],\end{aligned} \tag{25}$$

$$\begin{aligned}W(0)|_{k_s=1}=&\frac{\frac{1}{4}KA^2q^3}{\left(\cos^2\frac{\alpha}{2}+k_3\sin^2\frac{\alpha}{2}\right)^{3/2}}\Bigg[6\sin^4\frac{\alpha}{2}\left(2-3\sin^2\frac{\alpha}{2}\right)k_3^2\\&+2\sin^2\frac{\alpha}{2}\left(18\sin^4\frac{\alpha}{2}-26\sin^2\frac{\alpha}{2}+9\right)k_3\\&-18\sin^6\frac{\alpha}{2}+40\sin^4\frac{\alpha}{2}-26\sin^2\frac{\alpha}{2}+4\Bigg],\end{aligned} \tag{26}$$

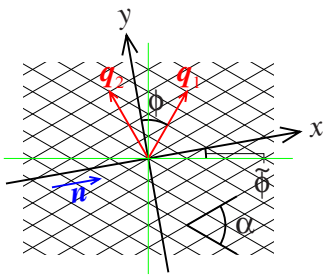

FIG. 6. (Color online) Illustration of the geometry of a surface with rhombic grooves. Thin green lines, diagonal lines of the rhombi, correspond to $\tilde{\phi}=0$ or $\tilde{\phi}=\pi/2$.

and again the values of $W(\pi/2)$ at $k_s=0$, 1, and 2 can be deduced from Eqs. (25), (26), and (24).

We can show from Eqs. (25) and (26) that when $\alpha \leq 2\arcsin(\sqrt{2}/3)$, or $\alpha \leq 56.25°$ in degrees, $W(0) \geq 0$ irrespective of the values of k_3 and k_s. The detail of its proof is given in Appendix A. When $\alpha > 56.25°$, it depends on k_3 and k_s whether $W(0)$ is positive or negative, as we have already seen in Sec. III B for $\alpha=\pi/2$. In Fig. 7, we show different phase diagrams for $\alpha=\pi/3$ (60°) and $5\pi/12$ (75°). As we can readily expect, the size of the region for negative $W(0)$ becomes smaller with smaller α.

The behavior of $W(\pi/2)$ can be classified to several regimes depending on α, which are summarized in Fig. 8. (i) When $2\arccos(\sqrt{6}/3) < \alpha \leq \pi/2$ (or $70.53° < \alpha \leq 90°$ in degrees), $W(\pi/2)$ can be positive when k_3 is larger than a certain value, irrespective of the value of k_s [Fig. 8(a)]. Notice

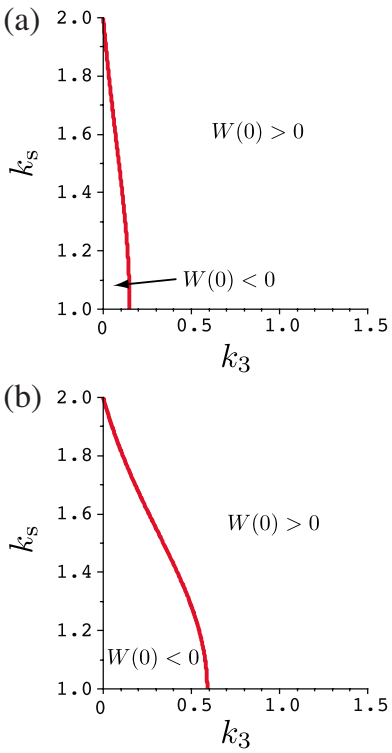

FIG. 7. (Color online) Phase diagrams for $W(0)$ of rhombic grooves with (a) $\alpha=\pi/3$ and (b) $\alpha=5\pi/12$.

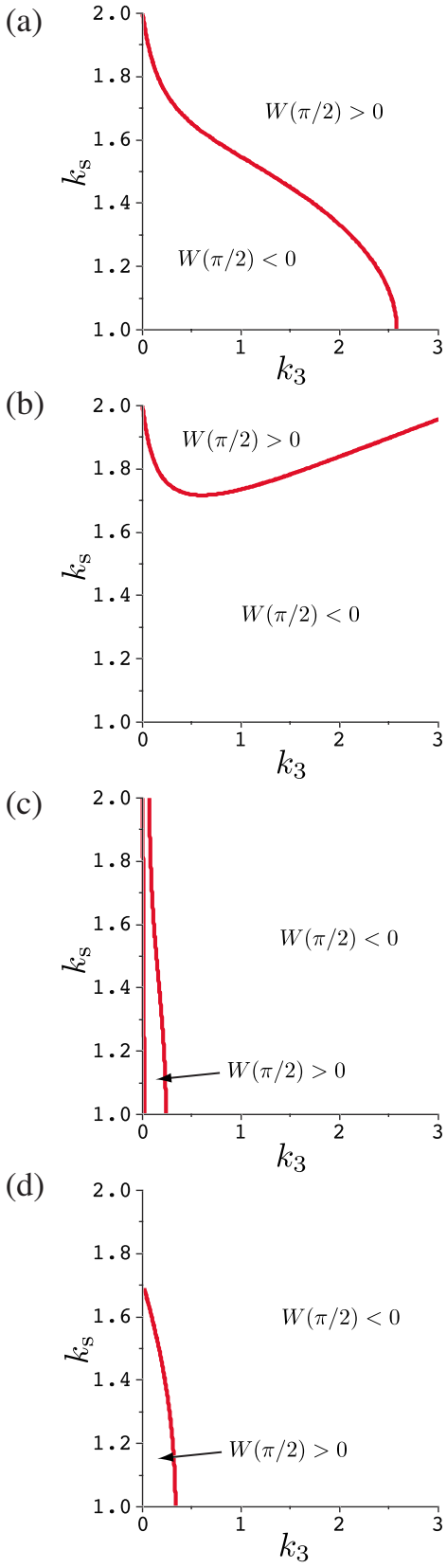

FIG. 8. (Color online) Phase diagrams for $W(\pi/2)$ of rhombic grooves with (a) $\alpha=5\pi/12$, (b) $\alpha=3\pi/8$, (c) $\alpha=\pi/8$, and (d) $\alpha=0$. Notice that in (c), there exist a very narrow region around $k_3 \simeq 0$, in which $W(\pi/2) < 0$.

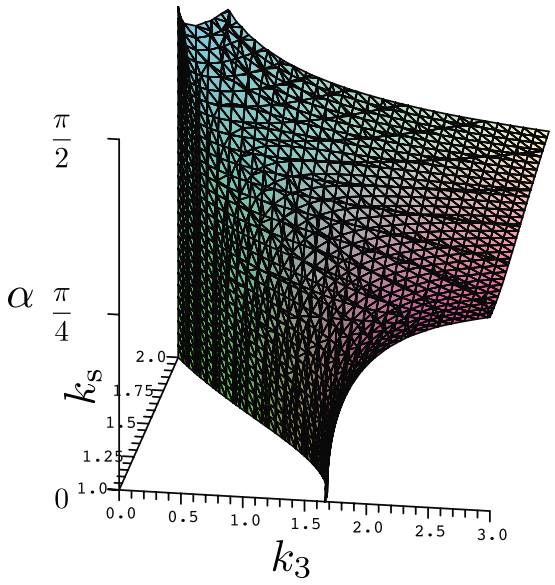

FIG. 9. (Color online) Implicit plot of $c(\alpha,k3,ks)=0$ or $\partial W(0)/\partial\alpha=0$ for $0<\alpha\leq\pi/2$.

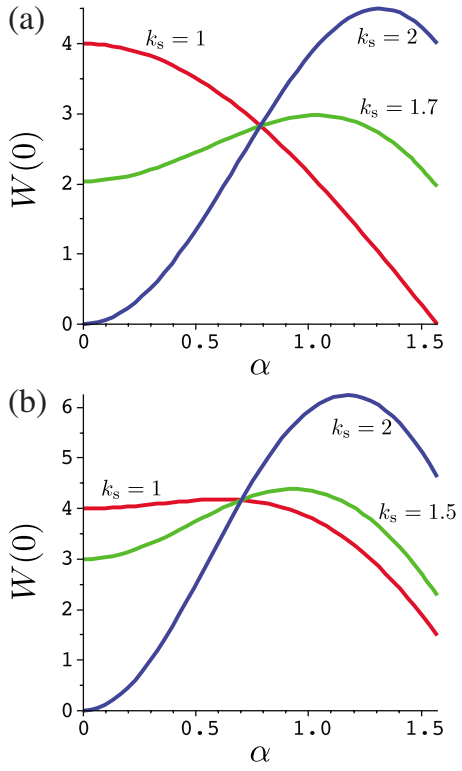

FIG. 10. (Color online) Plots of $W(0)$ as a function of α for (a) $k_3=1$ and (b) $k_3=2$.

that when $k_s=0$ or 2, $W(\pi/2)\geq 0$ is always satisfied. (ii) When $2\arccos(\sqrt{546+52\sqrt{3}}/26)<\alpha<2\arccos(\sqrt{6}/3)$ (or $28.13°<\alpha<70.53°$ in degrees), there exists a certain range of k_s in which $W(\pi/2)<0$ irrespective of the value of k_3. Otherwise, $W(\pi/2)>0$ in a certain finite range of k_3 [Fig. 8(b)]. (iii) When $0°<\alpha<28.13°$, irrespective of the value of k_s, there exists a certain finite range of k_3 in which $W(\pi/2)>0$ [Fig. 8(c)]. Mathematical details to arrive at those results are given in Appendix B.

Figure 8(d) presents a limiting case of $\alpha=0$. For $\alpha=0$, $W(\pi/2)$ is explicitly written as

$$W(\pi/2)|_{\alpha=0}=-\frac{2}{\sqrt{k_3}}[3k_3-1+2(k_s-1)^2], \tag{27}$$

and therefore $W(\pi/2)$ can be positive in a certain region of the phase diagram included in $k_3<1/3$ and $|k_s-1|<\sqrt{2}/2$. This result looks somewhat surprising, because in fact $\alpha=0$ corresponds to a "one-dimensional" groove, and $W(\pi/2)>0$ implies that director orientation perpendicular to the one-dimensional groove can be (meta)stable rather than unstable. As has already been pointed out in Ref. [34], positive $W(\pi/2)$ in the case of one-dimensional groove can be understood as follows: a nematic liquid crystal oriented perpendicular to the grooves involves bend and splay deformations, but no twist deformation. Saddle-splay surface elastic energy is also zero. Deviation of the nematic orientation from perpendicular alignment yields twist deformation, nonzero saddle-splay surface elastic energy, and reduced bend and splay elastic energies. However, if k_3 is small enough, the reduction in the bend elastic energy is too small to compensate for the twist elastic energy and the saddle-splay surface elastic energy, resulting in the increase in the total elastic energy, which implies $W(\pi/2)>0$. It is readily seen from Eq. (22) with $\alpha=0$, the increase in the elastic energy other than the bend energy is proportional to $k_s(2-k_s)$, and therefore the above qualitative argument holds only when $k_s(2-k_s)$ is large enough, that is, $|k_s-1|$ is small enough.

We conclude this section by finding out which α gives the largest anchoring strength $W(0)$ for given k_3 and k_s. For this purpose, we calculate $\partial W(0)/\partial\alpha$ to obtain

$$\frac{\partial W(0)}{\partial\alpha}=\frac{1}{4}KA^2q^3\frac{\cos\frac{\alpha}{2}\sin\frac{\alpha}{2}c(\alpha,k3,k_s)}{\left(\cos^2\frac{\alpha}{2}+k_3\sin^2\frac{\alpha}{2}\right)^{7/2}}, \tag{28}$$

with

$$\begin{aligned}c(\alpha,k3,k_s)=k_3\Bigg(&24+8(3k_3-11)\sin^2\frac{\alpha}{2}+(21k_3-137)(k_3-1)\\&\times\sin^4\frac{\alpha}{2}+2(k_3-1)^2(3k_3-50)\sin^6\frac{\alpha}{2}\\&-27(k_3-1)^3\sin^8\frac{\alpha}{2}\Bigg)+k_s(2-k_s)\Bigg(4(3k_3-5)\\&+(3k_3^2-26k_3+87)\sin^2\frac{\alpha}{2}-(k_3-1)(25k_3-141)\\&\times\sin^4\frac{\alpha}{2}-7(k_3-1)^2(7k_3-101)\sin^6\frac{\alpha}{2}\\&+27(k_3-1)^3\sin^8\frac{\alpha}{2}\Bigg).\end{aligned} \tag{29}$$

It is clear from Eq. (28) that $\alpha=0$ yields $\partial W(0)/\partial\alpha=0$. As we shall see, $\alpha=0$, i.e., one-dimensional grooves, gives maximum $W(0)$ in a certain region in the (k_3,k_s) space, while outside the region it does not; $\alpha\neq 0$ result in maximum $W(0)$.

In Fig. 9, we present an implicit plot of $c(\alpha,k3,ks)=0$, that is, we plot α in $0<\alpha\leq\pi/2$ that gives $\partial W(0)/\partial\alpha=0$, as a function of k_3 and k_s. Figure 9 clearly demonstrates that orthogonal grooves, $\alpha=\pi/2$, does not necessarily result in maximum anchoring strength $W(0)$. In Fig. 10, we plot $W(0)$ as a function of α for several specific values of k_3 and k_s. In the case of $(k_3,k_s)=(1,1)$, for which $\alpha>0$ does not yield $\partial W(0)/\partial\alpha=0$ as seen in Fig. 9, $W(0)$ indeed attains its maximum at $\alpha=0$. On the other hand, in other cases presented in Fig. 10, the maximum of $W(0)$ is at α not equal to zero, which indicates that the value of α given by the manifold in Fig. 9 does yield the maximum, not the minimum, of $W(0)$. Thus, how to achieve largest anchoring strength $W(0)$ by rhombic grooves can be deduced from Fig. 9. One can also find from Fig. 10 that when $\alpha\neq 0$ gives the maximum of $W(0)$, $W(0)$ becomes larger for larger $|k_s-1|$. Therefore to attain large anchoring strength by rhombic grooves, one should use a nematic material with large K_{24}.

D. Hexagonally grooved surface and beyond: Surfaces with 2N-fold symmetry

Now we consider a grooved surface possessing $2N$-fold symmetry, in which the set of wave vectors $\{\boldsymbol{q}_m\}$ and $\{-\boldsymbol{q}_m\}$ with $m=0,1,\ldots,m-1$ are given by $\boldsymbol{q}_m=q[\sin(\phi+m\pi/N),\cos(\phi+m\pi/N)]$, and the amplitudes of those modulations are equal, $A=A_1=A_2=\cdots$ (see Fig. 11). Square grooves discussed in Sec. III B correspond to $N=2$. Again ϕ characterizes the orientation of the surface groove with respect to $\boldsymbol{n}$. We assume here $K_1=K_2=K$, and then the anchoring energy (15) is expressed in terms of $k_3=K_3/K$ and $k_s=K_s/K$ as

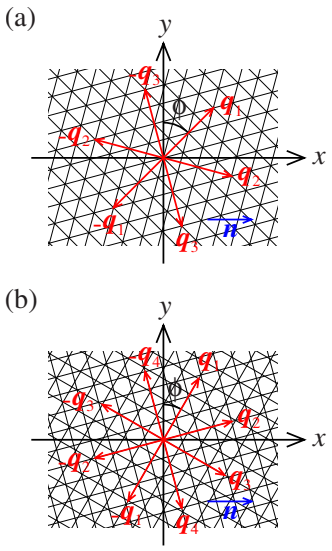

FIG. 11. (Color online) Illustration of the geometry of grooved surfaces with $2N$-fold symmetry: (a) $N=3$ (hexagonal) and (b) $N=4$. The angle ϕ can be understood as the angle between the director $\boldsymbol{n}$ (or the x axis) and the direction of one of the grooves (represented by thin solid black lines), as well as the angle between $\boldsymbol{q}_1$ and the y axis.

$$f=\frac{1}{4}KA^2q^3\sum_{m=0}^{N-1}\frac{k_3\sin^4\left(\phi+\frac{m\pi}{N}\right)+k_s(2-k_s)\cos^2\left(\phi+\frac{m\pi}{N}\right)\sin^2\left(\phi+\frac{m\pi}{N}\right)}{\sqrt{\cos^2\left(\phi+\frac{m\pi}{N}\right)+k_3\sin^2\left(\phi+\frac{m\pi}{N}\right)}}. \tag{30}$$

We first discuss a specific case of a hexagonally grooved surface $(N=3)$ in detail. We notice that when $k_3=1$, or $K_3=K(=K_1=K_2)$, f is independent of ϕ irrespective of the value of k_s, that is, the surface shows no azimuthal anchoring. This holds for arbitrary N larger than or equal to 3, and its derivation is given below.

For $K_3\neq K$, it is not difficult to show that $\partial f/\partial\phi=0$, at $\phi=n\pi/6$, with n being an integer. As in Sec. III B, we define $W(\phi)\equiv\partial^2 f/\partial\phi^2$ and discuss whether $f(n\pi/6)$ is the minimum or maximum of f. From Eq. (30) with $N=3$, we obtain

$$W(0)=\frac{1}{4}KA^2q^3\left(2k_s(2-k_s)+\frac{-k_s(2-k_s)(19+210k_3+27k_3^2)-27k_3(k_3-1)(3k_3+5)}{4(1+3k_3)^{5/2}}\right), \tag{31}$$

$$W(\pi/6)=\frac{1}{4}KA^2q^3\left(\frac{2k_s(2-k_s)-(3k_3+1)}{\sqrt{k_3}}-\frac{k_s(2-k_s)(19k_3^2+210k_3+27)-k_3(15k_3^2+122k_3+375)}{4(3+k_3)^{5/2}}\right). \tag{32}$$

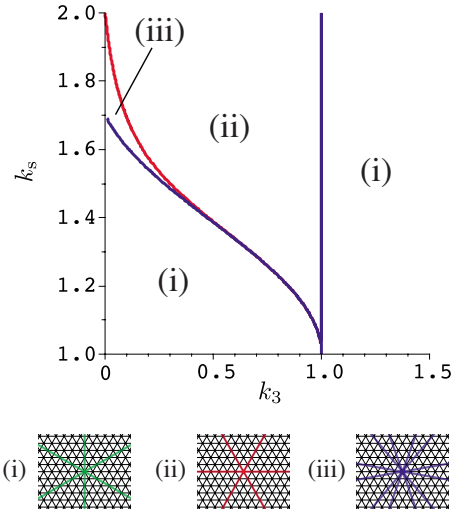

FIG. 12. (Color online) Phase diagram of a surface with hexagonal grooves. Schematic illustrations of the easy axes are also given. On the vertical line $k_3=1$, no azimuthal anchoring exists.

From symmetry it is clear that $W(0)=W(m\pi/3)$ and $W(\pi/6)=W(\pi/6+m\pi/3)$, with m being an arbitrary integer. It is easily verified that $W(0)=W(\pi/6)=0$ when $k_3=1$, which is a natural consequence of the absence of anchoring in the case of $k_3=1$ as noted above. We also find, with the aid of the algebraic program Maple 11, that $W(0)>0$ and $W(\pi/6)>0$ cannot be simultaneously satisfied. Therefore, just like the square grooves discussed in Sec. III B, we must consider the following three cases: (i) $W(0)<0$ and $W(\pi/6)>0$, (ii) $W(0)>0$ and $W(\pi/6)<0$, and (iii) $W(0)<0$ and $W(\pi/6)<0$. In case (i) three easy axes are along the directions $\phi=\pi/6$, $\pi/2$, and $5\pi/6$, and in case (ii) along $\phi=0$, $\pi/3$, and $2\pi/3$. In case (iii), there exists an angle ϕ_i in the range $(0,\pi/6)$ which satisfies $W(\phi_i)=0$. The minima of the anchoring energy f are then located at $\phi=\pm\phi_i+m\pi/3$, and therefore the system has four easy axes along $\phi=\pm\phi_i$, $\pi/3\pm\phi_i$, and $2\pi/3\pm\phi_i$ [36].

In Fig. 12, we plot a phase diagram of hexagonal grooves together with schematic illustrations of the easy axes for cases (i), (ii), and (iii). When $k_3>1$, we always find case (i) in the phase diagram. When $k_3<1$, as in the case of square grooves it depends on k_s which case is realized, but a qualitative form of the phase diagram is somewhat different from that of square grooves. One finds a line $k_3=1$ separating the region (i) and (ii), which is absent in the phase diagram of square grooves, and on which no azimuthal anchoring is present as noted above. For $k_s=1$, we observe case (i) irrespective of the value of k_3. Case (iii) is realized in a very narrow region in the phase diagram. Again case (i) is likely to be observed because for most rodlike nematic liquid crystal $k_3>1$.

We plot in Fig. 13 the ϕ dependence of the anchoring energy for various k_3 and k_s. Here again we use the rescaled anchoring energy $\tilde{f}(\phi)$ defined in Eq. (21). For $k_3=1.5>1$ [Fig. 13(a)], the minima of f are found at $\phi=\pi/6$, $\pi/2$, and $5\pi/6$ [corresponding to case (i)], irrespective of the value of k_s. For $k_3=0.7<1$, on the other hand, it depends on K_s where

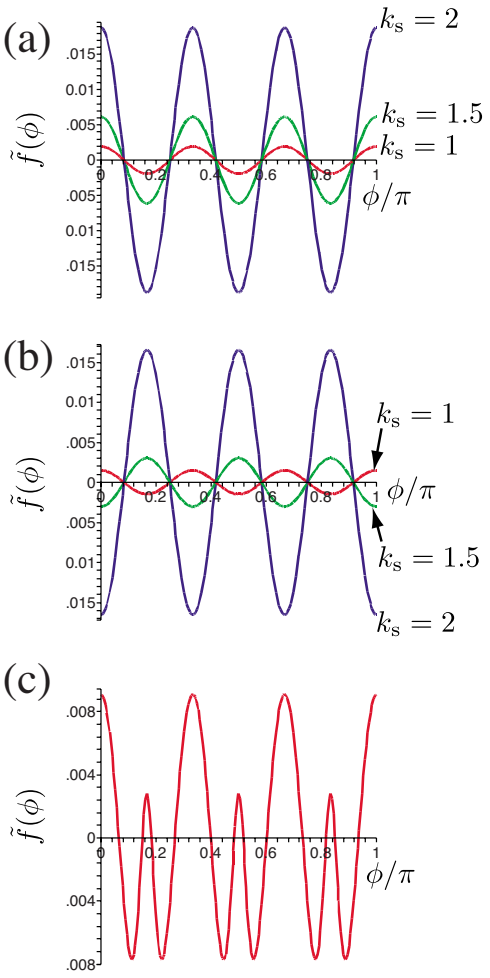

FIG. 13. (Color online) Plot of the rescaled anchoring energy $\tilde{f}(\phi)$ for (a) $k_3=1.5$, (b) $k_3=0.7$, and (c) $k_3=0.02$ and $k_s=1.8$.

the minima of f are located [Fig. 13(b)]; when $k_s=1$ the minima are at $\phi=\pi/6$, $\pi/2$, and $5\pi/6$, while for other values of k_s the minima are at $\phi=0$, $\pi/3$, and $2\pi/3$. Figure 13(c) corresponds to case (iii). Those behaviors of the anchoring energy are consistent with the phase diagram, Fig. 12.

Figure 14 shows the plot of the anchoring strengths $W(0)$ and $W(\pi/6)$ as a function of k_3 and k_s. We find from Fig. 14

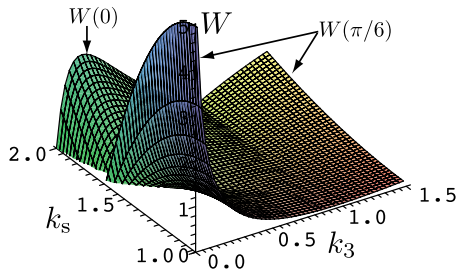

FIG. 14. (Color online) Plot of the anchoring strengths $W(0)$ and $W(\pi/6)$ as a function of k_3 and k_s for a surface with hexagonal grooves. Only the regions where $W(0)>0$ or $W(\pi/6)>0$ are shown.

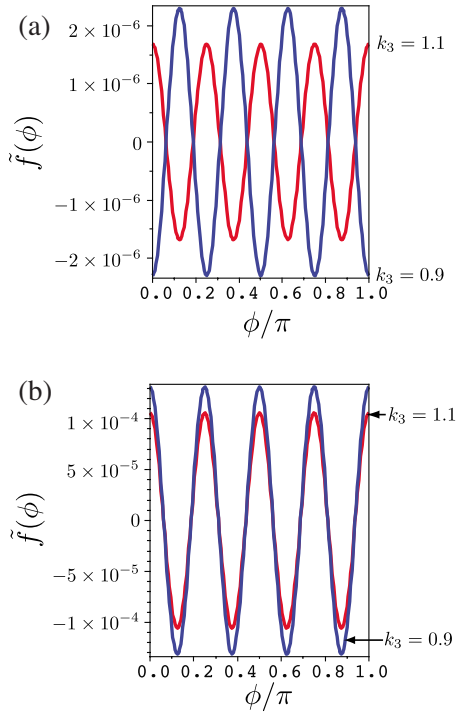

FIG. 15. (Color online) Plot of the rescaled anchoring energy $\tilde{f}(\phi)$ for $N=4$ and (a) $k_s=1$, and (b) $k_s=2$.

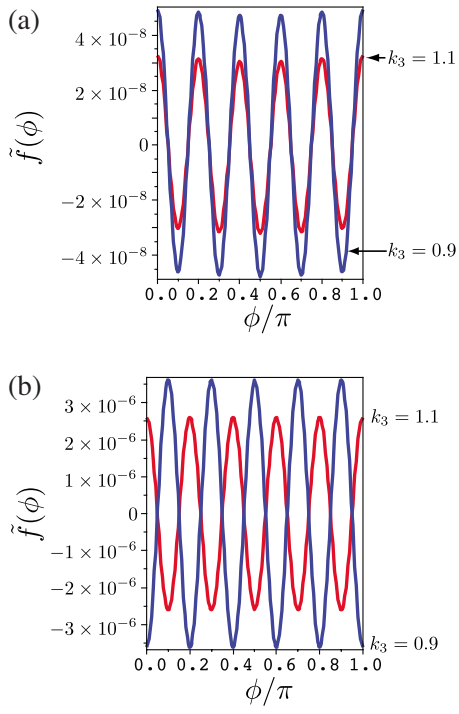

FIG. 16. (Color online) Plot of the rescaled anchoring energy $\tilde{f}(\phi)$ for $N=5$ and (a) $k_s=1$, and (b) $k_s=2$.

that in the region where $W(0)>0$, $W(0)$ becomes largest for fixed k_3 when $k_s=2$ (or 0). On the other hand, which k_s yields largest $W(\pi/6)$ depends on k_3; $k_s=2$ (or 0) when $k_3>1$, and $k_s=1$ when $k_3<1$. The absence of surface anchoring when $k_3=1$ is also seen from Fig. 14.

We conclude this section by noticing that we can show the following for general N:

(i) The anchoring energy f, Eq. (30), exhibits its extrema $(\partial f/\partial\phi=0)$ at $\phi=n\pi/2N$, with n being an arbitrary integer. This holds irrespective of whether $K_1=K_2$ or not. Its derivation is given in Appendix C.

(ii) When $K_1=K_2=K$ and $|k_3-1|=|K_3/K-1|\ll 1$, f can be written, apart from an uninteresting constant independent of ϕ, as

$$f=\frac{1}{4}KA^2q^3C(N)(k_3-1)^{N-2}[k_3-k_s(2-k_s)]\cos 2N\phi + O((k_3-1)^{N-1}), \tag{33}$$

for $k_s(2-k_s)\neq 1$. In Eq. (33), we have defined a positive constant $C(N)\equiv N(2N-5)!!2^{3(N-1)}(N-2)!$ that depends only on N. When $k_s(2-k_s)=1$, Eq. (33) is replaced by

$$f=\frac{1}{4}KA^2q^3\frac{C(N)}{2(N-1)}(k_3-1)^{N-1}\cos 2N\phi+O((k_3-1)^N). \tag{34}$$

In particular, when $k_3=1$ and $N\geq 3$, Eq. (33) and (34) indicates, as we have stated above without giving a proof, that f is independent of ϕ; the surface exhibits no azimuthal anchoring. We give the proof of Eqs. (33) and (34) in Appendix D.

(iii) Using the previous results (33) and (34), we can investigate the direction of the easy axes (or the location of the minima in f), in the case of sufficiently small $|k_3-1|$. From Eq. (33), when $k_3>1$, the easy axes are along $\phi=(2n+1)\pi/2N$ irrespective of N, with n being an arbitrary integer [note that $k_3-k_s(2-k_s)$ in Eq. (33) is positive]. On the other hand, the direction of the easy axes depends sensitively on N and k_s when $k_3<1$, as we have already seen in the cases of $N=2$ and 3. When $k_s(2-k_s)$ is not close to 1 (that is, k_s itself is not close to 1), $k_3-k_s(2-k_s)$ can be assumed positive. Then from Eq. (33) they are along $\phi=(2n+1)\pi/2N$ for even N and $\phi=n\pi/N$ for odd N. When $k_s(2-k_s)\simeq 1$ (i.e., $k_s\simeq 1$), the positiveness of $k_3-k_s(2-k_s)$ in Eq. (33) is no longer assumed, and in the case of $k_s(2-k_s)=1$, we must use Eq. (34); the easy axes are along $\phi=(2n+1)\pi/2N$ for odd N and $\phi=n\pi/N$ for even N, opposite to what we have seen above when k_s is not close to 1.

We plot in Figs. 15 and 16, the rescaled anchoring energy defined by Eq. (21) for $N=4$ (Fig. 15) and $N=5$ (Fig. 16). In Figs. 15 and 16, we have chosen $k_3=1.1$ or 0.9, and $k_s=1$ or 2. When $k_3=1.1>0$, the minima of $\tilde{f}$ are located at $\phi=(2n+1)/8\pi$ $(N=4)$, or at $\phi=(2n+1)/10\pi$ $(N=5)$, with n being an arbitrary integer, irrespective of whether $k_s=1$ or 2. On the other hand, in the case of $k_3=0.9<1$, the location of the minima of $\tilde{f}$ depends on the value of k_s and whether N is even or odd. The behavior of the anchoring energy found in Figs. 15 and 16 agrees with the argument above.

IV. CONCLUSION

In our previous work [24–26] we argued that the pioneering study of Berreman on the surface anchoring of a sinusoidally grooved surface should be critically reexamined. In this paper we extended our theory to the anchoring of a nonflat surface of general shape. We considered the elastic distortion of the director field due to the undulation of the surface imposing local planar degenerate anchoring, and derived an analytic expression for the Frank elastic energy of the distorted nematic liquid crystal, or the anchoring energy due to a nonflat surface of arbitrary shape with sufficiently small surface slopes.

First we examined the anchoring energy of a one-dimensionally grooved surface. We showed that the reduced anchoring energy $f(\phi)/f(\pi/2)$ is independent of the shape of the surface. The previous findings for sinusoidal surfaces, therefore, hold for one-dimensional grooves of any shape. For example, in a simplified one-constant case ($K_1=K_2=K_3=K$), the anchoring strength of the Rapini-Papoular sense becomes zero when $K_s=0$ or $2K$ (that is, $|K_{24}|=K$), In that case the anchoring energy is proportional to $\sin^4\phi$. Berreman's original result, $f(\phi)\propto\sin^2\phi$ is correct only when $K_s=K$ (or $K_{24}=0$).

We extended our theory and applied it to two-dimensionally grooved surfaces. In a simple case of square grooves together with an assumption of $K_1=K_2=K$, we demonstrated that the direction of the easy axes depends crucially on $k_3\equiv K_3/K$ and $k_s\equiv K_s/K$. In the case of $k_3\geq 1$, the two diagonal directions always become stable, which yields bistability, except when $k_s=1$. When $k_3<1$, the direction of the easy axes is determined by k_s and k_3: Two easy axes can be along the diagonal lines or the sides of the squares depending on k_s and k_3, and even four easy axes can exist in some extreme cases. For fixed k_3, we also showed that when the easy axes are along the diagonal directions, $k_s=0$ or 2 yields the largest anchoring strength in the Rapini-Papoular sense. On the other hand, maximum anchoring strength is achieved at $k_s=1$ when the easy axes are along the sides of the squares.

We further considered how a surface with rhombic grooves behaves and examined the stability and the anchoring strength of the axes along the diagonal directions. It was found that the longer diagonal axis ($\tilde{\phi}=0$ in the notation of the text) is stable irrespective of the values of k_3 and k_s, when α, the angle between the sides of the rhombi, is smaller than 56.25°. The size of the region in the (k_3,k_s) space in which the longer diagonal axis becomes unstable is smaller as α approaches 56.25° from above. The stability of the shorter diagonal axis ($\tilde{\phi}=\pi/2$) depends on k_3, k_s, and α in a highly complicated manner. Irrespective of α there exists a certain set of k_3 and k_s which results in a (meta)stable shorter diagonal axis, even when $\alpha=0$, i.e., a shorter diagonal axis is along a direction orthogonal to one-dimensional grooves. We also examined which α gives the maximum anchoring strength along the longer diagonal axis. We found that in a certain region in the (k_3,k_s) space, $\alpha=0$ (i.e., one-dimensional grooves) yields the largest anchoring strength, while outside it the largest anchoring strength is achieved at finite and nonzero α that depends on k_3 and k_s. We presented in Fig. 9 how to obtain largest anchoring strength for a given nematic material.

We also investigated the anchoring of a grooved surface possessing $2N$-fold symmetry. We showed that such a surface with $N\geq 3$ cannot show azimuthal anchoring in the one-constant case, $K_1=K_2=K_3$, irrespective of the value of K_s (or K_{24}). Although general conclusions cannot be drawn from those small number of specific examples, it is likely that a surface with high symmetry could not be expected to yield azimuthal anchoring, in the case of one-constant elasticity. On the contrary, for surfaces with lower symmetry, say, one-dimensional grooves or rhombic grooves, one-constant elasticity does not lead to the absence of azimuthal anchoring as we have seen.

We presented a detailed argument on hexagonal grooves ($N=3$) with $k_3\neq 1$. In most cases the surface exhibits tristability, with the angle between two of the three easy axes being $\pi/3$. The direction of the easy axes with respect to the surface pattern is fixed (in the notation of the text, at $\phi=\pi/6$, $\pi/2$, and $5\pi/6$) when $k_3>1$, while it depends on k_3 and k_s when $k_3<1$. We also showed that six easy axes can exist in a very narrow region in the (k_3,k_s) space. In the cases of general N, the direction of the easy axes depends on whether N is even or odd, as well as on k_3 and k_s.

We conclude this paper by emphasizing again that our theoretical framework is applicable to a surface of arbitrary shape, so long as the surface slope is small enough and linear elasticity [Eq. (6)] is safely assumed. Considering the recent growing interest in the anchoring attributable to surface geometry, and an increasing number of attempts to manufacture grooved surfaces to achieve specific anchoring properties, we hope that our theoretical framework presented in this paper will help understand the properties of anchoring induced by surface geometry in a clearer and more quantitative manner, and propose surface shape that will lead to desired anchoring properties.

ACKNOWLEDGMENTS

This work is in part supported by KAKENHI (Grant-in-Aid for Scientific Research) on Priority Area "Soft Matter Physics" from the Ministry of Education, Culture, Sports, Science, and Technology of Japan.

APPENDIX A

Here we show that $W(0)$ for rhombic grooves, Eq. (23), is non-negative irrespective of the values of k_3 and k_s when $\alpha\leq 2\arcsin(\sqrt{2}/3)$. Since $W(0)$ is a linear function of $k_s(2-k_s)$, and $0\leq k_s(2-k_s)\leq 1$, to show the positiveness of $W(0)$ for given k_3 and α it is sufficient to verify $W(0)\geq 0$ at $k_s(2-k_s)=0$ and 1 [or $k_s=0$ (or 2) and 1].

It is easily shown that $W(0)|_{k_s=0 \text{ or } 2}$, or Eq. (25), is not negative irrespective of the values of k_3 and α (as long as $k_3\geq 0$ and $0\leq\alpha\leq\pi/2$ as we have postulated). To show this we rewrite Eq. (25) as

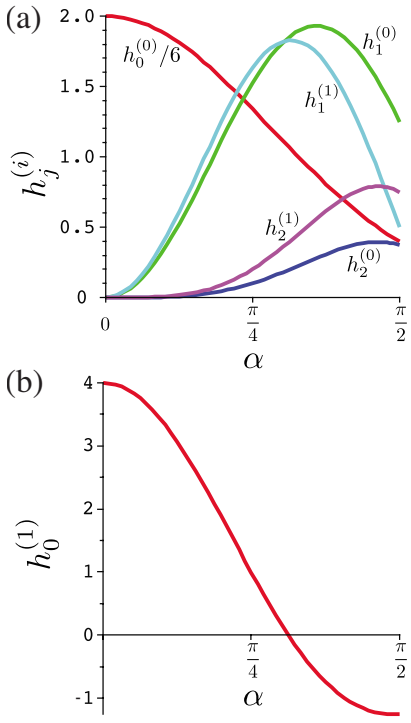

FIG. 17. (Color online) (a) Plot of $h_0^{(0)}/6$, $h_1^{(0)}$, $h_2^{(0)}$, $h_1^{(1)}$, and $h_2^{(1)}$ as a function of α to show their non-negativeness in the range $0 \le \alpha \le \pi/2$. (b) Plot of $h_0^{(1)}$ as a function of α. Note that $h_0^{(1)}(\alpha) = 0$ at $\alpha = 2\arcsin(\sqrt{2}/3) \simeq 0.982$.

$$W(0)|_{k_s=0 \text{ or } 2} = \frac{1}{4}KA^2q^3 \frac{2k_3 \sin^2\frac{\alpha}{2}\sum_{j=0}^{2} h_j^{(0)}(\alpha)k_3^j}{\left(\cos^2\frac{\alpha}{2} + k_3 \sin^2\frac{\alpha}{2}\right)^{5/2}}, \quad \text{(A1)}$$

where

$$h_0^{(0)}(\alpha) = -9\sin^6\frac{\alpha}{2} + 28\sin^4\frac{\alpha}{2} - 31\sin^2\frac{\alpha}{2} + 12,$$

$$h_1^{(0)}(\alpha) = \sin^2\frac{\alpha}{2}\left(18\sin^4\frac{\alpha}{2} - 34\sin^2\frac{\alpha}{2} + 15\right),$$

$$h_2^{(0)}(\alpha) = 3\sin^4\frac{\alpha}{2}\left(2 - 3\sin^2\frac{\alpha}{2}\right). \quad \text{(A2)}$$

As Fig. 17(a) clearly indicates, $h_0^{(0)}(\alpha), h_1^{(0)}(\alpha), h_2^{(0)}(\alpha) \ge 0$ for $0 \le \alpha \le \pi/2$, which yields $W(0)|_{k_s=0 \text{ or } 2} \ge 0$.

Similarly, we rewrite Eq. (26) as

$$W(0)|_{k_s=1} = \frac{1}{4}KA^2q^3 \frac{\sum_{j=0}^{2} h_j^{(1)}(\alpha)k_3^j}{\left(\cos^2\frac{\alpha}{2} + k_3 \sin^2\frac{\alpha}{2}\right)^{3/2}}, \quad \text{(A3)}$$

where

$$h_0^{(1)}(\alpha) = -18\sin^6\frac{\alpha}{2} + 40\sin^4\frac{\alpha}{2} - 26\sin^2\frac{\alpha}{2} + 4,$$

$$h_1^{(1)}(\alpha) = 2\sin^2\frac{\alpha}{2}\left(18\sin^4\frac{\alpha}{2} - 26\sin^2\frac{\alpha}{2} + 9\right),$$

$$h_2^{(1)}(\alpha) = 6\sin^4\frac{\alpha}{2}\left(2 - 3\sin^2\frac{\alpha}{2}\right) = 2h_2^{(0)}(\alpha). \quad \text{(A4)}$$

Again from Fig. 17(a), we find that $h_2^{(1)}(\alpha)$ and $h_1^{(1)}(\alpha)$ are not negative for $0 \le \alpha \le \pi/2$. We also find that $h_0^{(1)}(\alpha) \ge 0$ when $\alpha \le 2\arcsin(\sqrt{2}/3)$ and $h_0^{(1)} < 0$ when $\alpha > 2\arcsin(\sqrt{2}/3)$ [see Fig. 17(b)]. Therefore, when $\alpha \le 2\arcsin(\sqrt{2}/3)$, $W(0)|_{k_s=1} \ge 0$ for all $k_3 \ge 0$. Now we have shown that $W(0) \ge 0$ irrespective of the values of k_3 and k_s when $\alpha \le 2\arcsin(\sqrt{2}/3)$.

APPENDIX B

Here we examine how the anchoring strength $W(\pi/2)$ for rhombic grooves behaves with respect to the variation of α, k_3, and k_s. As in Appendix A, $W(\pi/2)$ is again a linear function of $k_s(2-k_s)$, and therefore investigation of the cases of $k_s(2-k_s) = 0$ and 1 will give sufficient information on the qualitative behavior of $W(\pi/2)$.

From Eqs. (24) and (A1),

$$W(\pi/2)|_{k_s=0 \text{ or } 2} = \frac{1}{4}KA^2q^3 \frac{2k_3 \cos^2\frac{\alpha}{2}\sum_{j=0}^{2} h_j^{(0)}(\pi-\alpha)k_3^j}{\left(\sin^2\frac{\alpha}{2} + k_3 \cos^2\frac{\alpha}{2}\right)^{5/2}}, \quad \text{(B1)}$$

where $h_j^{(0)}$ has been defined in Eq. (A2).

Since $h_0^{(0)}(\pi-\alpha) > 0$ for $0 < \alpha \le \pi/2$ [see Fig. 18(a)], $W(\pi/2)|_{k_s=0 \text{ or } 2}$ is always positive for $0 < \alpha \le \pi/2$ when k_3 is sufficiently small. We also find from Fig. 18(b) that $h_2^{(0)}(\pi-\alpha) > 0$ (or < 0) when $\alpha > 2\arccos(\sqrt{6}/3)$ [or $< 2\arccos(\sqrt{6}/3)$]. Therefore, when $\alpha < 2\arccos(\sqrt{6}/3)$, there exists a certain $\bar{k}_3$, which satisfies $W(\pi/2)|_{k_s=0 \text{ or } 2} > 0$ (or < 0) when $k_3 < \bar{k}_3$ (or $> \bar{k}_3$). On the other hand, $W(\pi/2)|_{k_s=0 \text{ or } 2}$ is positive irrespective of the value of k_3 when $\alpha > 2\arccos(\sqrt{6}/3)$ [notice that $h_1^{(0)}$ is positive in this range of α; see Fig. 18(b)].

Now we consider the case of $k_s = 1$. From Eqs. (24) and (A3), we have

$$W(\pi/2)|_{k_s=1} = \frac{1}{4}KA^2q^3 \frac{\sum_{j=0}^{2} h_j^{(1)}(\pi-\alpha)k_3^j}{\left(\sin^2\frac{\alpha}{2} + k_3 \cos^2\frac{\alpha}{2}\right)^{3/2}}, \quad \text{(B2)}$$

where $h_j^{(1)}$ is defined in Eq. (A4). We first notice from Fig. 19(a) that $h_0^{(1)} < 0$ for $0 < \alpha \le \pi/2$, which indicates that $W(\pi/2)|_{k_s=1}$ is negative for sufficiently small k_3. We also

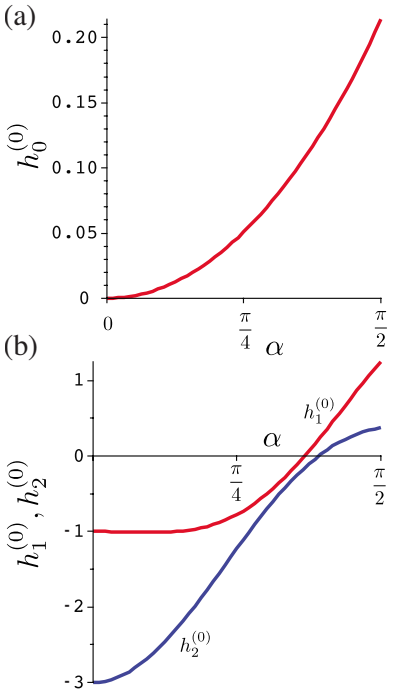

FIG. 18. (Color online) Plots of (a) $h_0^{(0)}(\pi-\alpha)$ and (b) $h_1^{(0)}(\pi-\alpha)$ and $h_2^{(0)}(\pi-\alpha)$ as a function of α. Note that $h_2^{(0)}(\pi-\alpha)$ becomes zero at $\alpha=2\arccos(\sqrt{6}/3)$.

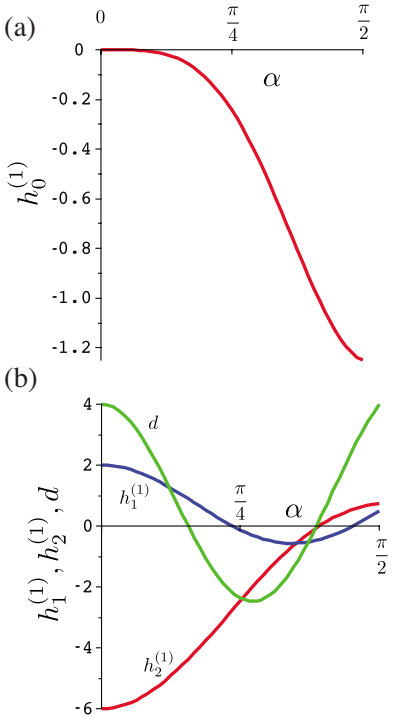

FIG. 19. (Color online) Plots of (a) $h_0^{(1)}(\pi-\alpha)$ and (b) $h_1^{(1)}(\pi-\alpha)$, $h_2^{(0)}(\pi-\alpha)$, and $d(\alpha)$ as a function of α. Note that $h_2^{(0)}(\pi-\alpha)$ becomes zero at $\alpha=2\arccos(\sqrt{6}/3)$ and that $d(\alpha)=0$ at $\alpha=2\arccos(\sqrt{546\pm52\sqrt{3}}/26)$.

note that $h_2^{(0)}(=2h_2^{(0)})>0$ (or <0) when $\alpha>2\arccos(\sqrt{6}/3)$ [or $<2\arccos(\sqrt{6}/3)$]; see Fig. 19(b). Together with $h_0^{(1)}<0$, we find that when $\alpha>2\arccos(\sqrt{6}/3)$, there exists a certain $\bar{k}_3$, which satisfies $W(\pi/2)|_{k_s=1}>0$ (or <0) when $k_3>\bar{k}_3$ (or $<\bar{k}_3$).

The behavior of $W(\pi/2)|_{k_s=1}$ in the case of $h_2^{(0)}<0$ [or $<2\arccos(\sqrt{6}/3)$] depends critically on the discriminant defined by

$$d(\alpha) \equiv [h_1^{(1)}(\pi-\alpha)]^2 - 4h_0^{(1)}(\pi-\alpha)h_2^{(1)}(\pi-\alpha). \quad \text{(B3)}$$

When

$$2\arccos(\sqrt{546+52\sqrt{3}}/26) < \alpha < 2\arccos(\sqrt{546-52\sqrt{3}}/26),$$

$d(\alpha)<0$ [see Fig. 19(b)], which implies that $W(\pi/2)|_{k_s=1}$ is negative for all k_3. When $2\arccos(\sqrt{546-52\sqrt{3}}/26)<\alpha<2\arccos(\sqrt{6}/3)$, formally $W(\pi/2)|_{k_s=1}=0$ has real solutions as an equation for k_3. But since $h_1^{(1)}(\pi-\alpha)<0$ in this range of α from Fig. 19(b), those solutions are negative, which indicates that $W(\pi/2)|_{k_s=1}$ is negative for all $k_3>0$. On the other hand, in the case of $0<\alpha<2\arccos(\sqrt{546+52\sqrt{3}}/26)$, $d(\alpha)>0$ and $h^{(1)}(\pi-\alpha)>0$ from Fig. 19(b), which implies that $W(\pi/2)|_{k_s=1}=0$ has two positive solutions as an equation of k_3. Therefore, $W(\pi/2)|_{k_s=1}$ is positive in a certain range of k_3.

The behavior of $W(\pi/2)|_{k_s=1}$ with the variation of α is thus summarized as follows: (i) when $2\arccos(\sqrt{6}/3)<\alpha\leq\pi/2$, $W(\pi/2)|_{k_s=1}$ is positive when k_3 is larger than a certain value; (ii) when $2\arccos(\sqrt{546+52\sqrt{3}}/26)<\alpha<2\arccos(\sqrt{6}/3)$, $W(\pi/2)|_{k_s=1}$ is negative for all $k_3>0$; (iii) when $0\leq\alpha<2\arccos(\sqrt{546+52\sqrt{3}}/26)$, $W(\pi/2)|_{k_s=1}$ is positive in a certain finite range of k_3.

These properties of $W(\pi/2)|_{k_s=0 \text{ or } 2}$ and $W(\pi/2)|_{k_s=1}$ result in the phase diagrams presented in Fig. 8.

APPENDIX C

Here we show that the anchoring energy described by Eq. (30), or the corresponding energy when $K_1\neq K_2$, satisfies $\partial f/\partial\phi=0$ at $\phi=n\pi/2N$ (n, arbitrary integer). It is obvious from symmetry that $f(\phi)=f(\phi+n\pi/N)$, and therefore it is sufficient to show $\partial f/\partial\phi=0$ at $\phi=0$ and $\phi=\pi/2N$.

From Eq. (14) with our choice of $\{\boldsymbol{q}_i\}$, the anchoring energy is written formally as

$$f(\phi) = \frac{1}{4}A^2q^3\sum_{m=0}^{N-1}\tilde{f}[\sin^2(\phi+m\pi/N)], \quad \text{(C1)}$$

where

$$\tilde{f}(\sin^2\phi) = K_3\frac{\sin^4\phi}{g_1(\phi)} + K_s\frac{(1-\sin^2\phi)\sin^2\phi}{g_1(\phi)} \times\left(2-\frac{K_s\,g_1(\phi)g_2(\phi)+\sin^2\phi-1}{K_3\sin^2\phi}\right), \quad \text{(C2)}$$

although the explicit form of $\tilde{f}$ is not important here. Note that $g_1(\phi)$ and $g_2(\phi)$ are rewritten as a function of $\sin^2\phi$.

The differentiation of Eq. (C1) with respect to ϕ yields

$$f'(\phi) \equiv \frac{\partial f(\phi)}{\partial \phi} = \frac{1}{2}A^2q^3\sum_{m=0}^{N-1}\tilde{h}(\phi + m\pi/N), \tag{C3}$$

where

$$\tilde{h}(\phi + m\pi/N) \equiv \tilde{f}'[\sin^2(\phi + m\pi/N)]\sin(\phi + m\pi/N) \times\cos(\phi + m\pi/N), \tag{C4}$$

in which $\tilde{f}'(x)$ implies $d\tilde{f}(x)/dx$.

It is easily shown from Eq. (C4) that $h(m\pi/N) = -h[(N-m)\pi/N]$ $(\phi=0)$. Then from Eq. (C3), we obtain

$$f'(0) = \frac{1}{2}A^2q^3\begin{cases}\tilde{h}(0) & (N,\ \text{odd}),\\ [\tilde{h}(0) + \tilde{h}(\pi/2)] & (N,\ \text{even}).\end{cases} \tag{C5}$$

It is easily found from Eq. (C4) that $\tilde{h}(0) = \tilde{h}(\pi/2) = 0$, and therefore we have shown $f'(0) = 0$.

When $\phi = \pi/2N$, Eq. (C4) yields $\tilde{h}(\pi/2N + m\pi/N) = -\tilde{h}[\pi/2N + (N-m-1)\pi/N]$, which results directly in $f'(\pi/2N) = 0$ for even N. For odd N, the only term that does not cancel out is the one with $m = (N-1)/2$, and therefore $f'(\pi/2N) = \frac{1}{2}A^2q^3\tilde{h}(\pi/2) = 0$. Finally we have shown $f'(\pi/2N) = 0$.

APPENDIX D

To derive Eqs. (33) and (34), using the expansion $1/\sqrt{1+x} = \Sigma_{\mu=0}^{\infty}(-1)^{\mu}\frac{(2\mu-1)!!}{\mu!2^{\mu}}x^{\mu}$ (see, e.g., p. 25 of Ref. [37]), we rewrite Eq. (30) as

$$f = \frac{1}{4}KA^2q^3\sum_{\mu=0}^{\infty}(-1)^{\mu}\frac{(2\mu-1)!!}{\mu!2^{\mu}}(k_3-1)^{\mu} \times\left[k_s(2-k_s)\sum_{m=0}^{N-1}\sin^{2(\mu+1)}\left(\phi + \frac{m\pi}{N}\right) + [k_3 - k_s(2-k_s)]\sum_{m=0}^{N-1}\sin^{2(\mu+2)}\left(\phi + \frac{m\pi}{N}\right)\right]. \tag{D1}$$

We first show that for a positive integer l with $l \le N-1$,

$$\sum_{m=0}^{N-1}\cos 2l\left(\phi + \frac{m\pi}{N}\right) = 0. \tag{D2}$$

Noticing the identity $\Sigma_{k=0}^{n-1}\cos(x+ky) = \cos\left(x + \frac{n-1}{2}y\right)\sin\frac{ny}{2}/\sin\frac{y}{2}$ (see, e.g., p. 35 of Ref. [37]), we obtain

$$\sum_{m=0}^{N-1}\cos 2l\left(\phi + \frac{m\pi}{N}\right) = \cos\left(2l\phi + \frac{(N-1)l\pi}{N}\right)\frac{\sin l\pi}{\sin\frac{l\pi}{N}}. \tag{D3}$$

For positive l with $l \le N-1$, $0 < l\pi/N < \pi$ and therefore $\sin\frac{l\pi}{N} \neq 0$. On the other hand, $\sin l\pi = 0$, which yields Eq. (D2).

We further show that

$$\sum_{m=0}^{N-1}\sin^{2\rho}\left(\phi + \frac{m\pi}{N}\right) = \begin{cases}\text{independent of } \phi & (\rho \le N-1),\\ \frac{N}{2^{2N}}\binom{2N}{N} + (-1)^N\frac{N}{2^{2N-1}}\cos 2N\phi & (\rho = N).\end{cases} \tag{D4}$$

For the derivation of Eq. (D4), one can use is the following identity (see, e.g., p. 30 of Ref. [37]) together with Eq. (D2),

$$\sum_{m=0}^{N-1}\sin^{2\rho}\left(\phi + \frac{m\pi}{N}\right) = \frac{N}{2^{2\rho}}\binom{2\rho}{\rho} + \frac{1}{2^{2\rho-1}}\sum_{\lambda=0}^{\rho-1}(-1)^{\rho-\lambda}\binom{2\rho}{\lambda} \times\sum_{m=0}^{N-1}\cos\left[2(\rho-\lambda)\left(\phi + \frac{m\pi}{N}\right)\right]. \tag{D5}$$

Equations (D1) and (D4) yield Eq. (33) for $k_s(2-k_s) \neq 1$ and Eq. (34) otherwise.

[1] P. G. de Gennes and J. Prost, *The Physics of Liquid Crystals*, 2nd ed. (Oxford University Press, Oxford, 1993).

[2] J. A. Castellano, Mol. Cryst. Liq. Cryst. **94**, 33 (1983).

[3] H. Yokoyama, in *Handbook of Liquid Crystal Research*, edited by P. J. Collings and J. S. Patel (Oxford University Press, Oxford, 1997), Chap. 6.

[4] J. Cheng and G. D. Boyd, Appl. Phys. Lett. **35**, 444 (1979).

[5] J. M. Geary, J. W. Goodby, A. R. Kmetz, and J. S. Patel, J. Appl. Phys. **62**, 4100 (1987).

[6] S. Ishihara, H. Wakemoto, K. Nakazima, and Y. Matsuo, Liq. Cryst. **4**, 669 (1989).

[7] M. Rüetschi, P. Grütter, J. Fünfschilling, and H.-J. Güntherodt, Science **265**, 512 (1994).

[8] B. Wen, M. P. Mahajan, and C. Rosenblatt, Appl. Phys. Lett. **76**, 1240 (2000); B. Wen and C. Rosenblatt, J. Appl. Phys. **89**, 4747 (2001).

[9] J.-H. Kim, M. Yoneya, J. Yamamoto, and H. Yokoyama, Appl. Phys. Lett. **78**, 3055 (2001); J.-H. Kim, M. Yoneya, and H. Yokoyama, Nature (London) **420**, 159 (2002).

[10] B. Zhang, F. K. Lee, O. K. C. Tsui, and P. Sheng, Phys. Rev. Lett. **91**, 215501 (2003).

[11] F. K. Lee, B. Zhang, P. Sheng, H. S. Kwok, and O. K. C. Tsui, Appl. Phys. Lett. **85**, 5556 (2004).

[12] M. Honma, K. Yamamoto, and T. Nose, J. Appl. Phys. **96**,

5415 (2004).
[13] S. Varghese, G. P. Crawford, C. W. M. Bastiaansen, D. K. G. de Boer, and D. J. Broer, Appl. Phys. Lett. **86**, 181914 (2005).
[14] J. S. Gwag, M. Yoneya, and H. Yokoyama, *IDW '06* (Otsu, Japan, 2006), p. LCT7-4L; J. S. Gwag, J. Fukuda, M. Yoneya, and H. Yokoyama, Appl. Phys. Lett. **91**, 073504 (2007); J. S. Gwag, M. Oh-e, M. Yoneya, H. Yokoyama, H. Satou, and S. Itami, J. Appl. Phys. **102**, 063501 (2007).
[15] F. S. Yeung and H. S. Kwok, Appl. Phys. Lett. **88**, 063505 (2006); F. S. Yeung, J. Y. Ho, Y. W. Li, F. C. Xie, O. K. Tsui, P. Sheng, and H. S. Kwok, *ibid.* **88**, 051910 (2006).
[16] D. W. Berreman, Phys. Rev. Lett. **28**, 1683 (1972); Mol. Cryst. Liq. Cryst. **23**, 215 (1973); see also Ref. [1], p. 115.
[17] S. Faetti, Phys. Rev. A **36**, 408 (1987).
[18] G. P. Bryan-Brown, M. J. Towler, M. S. Bancroft, and D. G. McDonnell, *Proceedings of International Display Research Conference* (Society for Information Display, California, 2004), p. 209.
[19] J.-B. Fournier and P. Galatola, Phys. Rev. E **60**, 2404 (1999).
[20] J. Elgeti and F. Schmid, Eur. Phys. J. E **18**, 407 (2005).
[21] E. S. Lee, P. Better, T. Miyashita, T. Uchida, M. Kano, M. Abe, and K. Sugawara, Jpn. J. Appl. Phys., Part 2 **32**, L1436 (1993).
[22] C. J. Newsome, M. O'Neill, R. J. Farley, and G. P. Bryan-Brown, Appl. Phys. Lett. **72**, 2078 (1998).
[23] R. Barberi, I. Dozov, M. Giocondo, M. Iovane, Ph. Martinot-Lagarde, D. Stoenescu, S. Tonchev, and L. V. Tsonev, Eur. Phys. J. B **6**, 83 (1998).
[24] J. Fukuda, M. Yoneya, and H. Yokoyama, Phys. Rev. Lett. **98**, 187803 (2007).
[25] J. Fukuda, M. Yoneya, and H. Yokoyama, Phys. Rev. Lett. **99**, 139902(E) (2007).
[26] J. Fukuda, M. Yoneya, and H. Yokoyama (unpublished).
[27] S. Chandrasekhar, *Liquid Crystals*, 2nd ed. (Cambridge University Press, Cambridge, 1992).
[28] E. G. Virga, *Variational Theories for Liquid Crystals* (Chapman and Hall, London, 1994).
[29] J. Nehring and A. Saupe, J. Chem. Phys. **54**, 337 (1971).
[30] C. Oldano and G. Barbero, Phys. Lett. **110A**, 213 (1985); J. Physiol. (Paris) **46**, 451 (1985).
[31] H. Yokoyama, Phys. Rev. E **55**, 2938 (1997).
[32] C. P. Crawford, in *Physical Properties of Liquid Crystals: Nematics*, edited by D. A. Dunmer, A. Fukuda, and G. R. Luckhurst (Institution of Electrical Engineers, London, 2001).
[33] J. L. Ericksen, Phys. Fluids **9**, 1205 (1966).
[34] U. Wolff, W. Greubel, and H. Krüger, Mol. Cryst. Liq. Cryst. **23**, 187 (1973).
[35] A. Rapini and M. Papoular, J. Phys. (Paris), Colloq. **30**, C4 (1969).
[36] To be strict, we cannot rule out the possibilities that $\partial f/\partial\phi=0$ has solutions other than $\phi=n\pi/4$ (square grooves) or $\phi=n\pi/6$ (hexagonal grooves) in cases (i) and (ii), and that $\partial f/\partial\phi=0$ has two or more solutions in the range $(0,\pi/4)$ (square grooves) or $(0,\pi/6)$ (hexagonal grooves) in case (iii). However, we have not found such unusual cases.
[37] I. S. Gradshteyn and I. M. Ryzhik, *Tables of Integrals, Series, and Products*, 6th ed. (Academic, London, 2000).